HAL
open science

# From femtosecond infrared to picosecond visible pulses: temporal shaping with high-efficiency conversion

Matteo Conforti, Fabio Baronio, Costantino De Angelis

## To cite this version:

Matteo Conforti, Fabio Baronio, Costantino De Angelis. From femtosecond infrared to picosecond visible pulses: temporal shaping with high-efficiency conversion. Optics Letters, 2007, 32 (13), pp.1779-1781. 10.1364/OL.32.001779 . hal-02405088

**HAL Id: hal-02405088**

**https://hal.science/hal-02405088v1**

Submitted on 11 Dec 2019

**HAL** is a multi-disciplinary open access archive for the deposit and dissemination of scientific research documents, whether they are published or not. The documents may come from teaching and research institutions in France or abroad, or from public or private research centers.

L'archive ouverte pluridisciplinaire **HAL**, est destinée au dépôt et à la diffusion de documents scientifiques de niveau recherche, publiés ou non, émanant des établissements d'enseignement et de recherche français ou étrangers, des laboratoires publics ou privés.

# From femtosecond infrared to picosecond visible pulses: temporal shaping with high efficiency conversion

**Matteo Conforti, Fabio Baronio, and Costantino De Angelis**

*Dipartimento di Elettronica per l'Automazione, Università di Brescia, via Branze 38, 25123 Brescia, Italy*

Compiled April 18, 2007

We present a single-pass frequency doubler that efficiently converts broadband near-infrared femtosecond pulses into narrow-spectrum visible picosecond pulses. An optimal control technique is introduced for properly designing aperiodically poled nonlinear crystals to generate visible pulses of the desired amplitude, phase profile, and carrier wavelength. © 2007 Optical Society of America

*OCIS codes:* 190.2620, 190.7110, 320.5540.

Visible picosecond pulsed laser radiation of the desired amplitude, phase profile, and carrier wavelength is desirable in a broad range of contexts, from condensed-matter spectroscopy to biological imaging, from metrology to industrial test applications.[1] Nowadays tunable sources of femtosecond pulses are easily available, whereas the generation of picosecond pulses requires complex setups.[1] Conventional gas laser sources in the visible range typically exhibit only discrete wavelength emission. Nonlinear frequency conversion schemes may be exploited to produce variable-wavelength visible radiation, in the absence of suitable laser gain media: up-conversion of the infrared radiation from optical parametric oscillators via intracavity or extracavity sum-frequency mixing and second-harmonic generation,[2] or down-conversion of ultraviolet sources via optical parametric oscillation and generation.[3] In general, these setups are relatively complicated and expensive. Alternatively, devices that combine a femtosecond fiber-based near infrared source and a subsequent single-pass frequency doubler can efficiently provide widely tunable picosecond pulsed radiation from blue to red.[4] In this Letter we propose a single-pass frequency doubler device that converts broadband near-infrared femtosecond pulses into narrow-spectrum visible pulses with i) a tunable carrier wavelength, ii) the desired amplitude and phase profile and iii) high efficiency conversion ($> 50\%$). To this end, we introduce an optimal pulse shaping control technique for properly designing aperiodically poled ferroelectric crystals capable of producing the desired visible pulsed radiation.

The literature on pulse shaping by second-harmonic generation is quite rich, but usually severe assumptions are taken. The case of negligible pump depletion was thoroughly studied, with particular emphasis on pulse compression and using linearly chirped gratings, by Fejer and co-workers.[5] More recently the issue of arbitrary pulse shaping was solved by means of simulated annealing.[6] However both these approaches are valid for conversion efficiencies of only a few percent. An alternative and elegant approach based on optimal control,[7]permits the limitation of pump-depletion to be overcome. However the cited method works only for real fields, so that that both group velocity dispersion and phase mismatch have to be neglected and only constant-phase pulses can be shaped (note that this fact also precludes wavelength tunability). In the following we extend in a nontrivial way this approach in order to take into account all the above mentioned effects.

In the process of second harmonic generation in a non uniform quasi-phase-matching (QPM) structure, the coupled nonlinear partial differential equations governing the propagation of the complex electric field amplitudes $E_m(z,t)$ ($m = 1$ fundamental field FF, $m = 2$ second harmonic field SH) of two plane waves of central frequencies $\omega_m$ ($\omega_2 = 2\omega_1$) and wave numbers $k_m$ travelling along the $z$ axis read:

$$\begin{aligned} i\frac{\partial E_1}{\partial z} &= \frac{\beta_1}{2}\frac{\partial^2 E_1}{\partial t^2} - G(z)\exp(-i\Delta k z)E_1^* E_2, \qquad (1)\\ i\frac{\partial E_2}{\partial z} &= i\delta\frac{\partial E_2}{\partial t} + \frac{\beta_2}{2}\frac{\partial^2 E_2}{\partial t^2} - G(z)\exp(i\Delta k z)E_1^2, \end{aligned}$$

with $\Delta k = 2k_1 - k_2$ the wave number mismatch, $\delta$ the difference between the inverse group velocity at FF and SH, $\beta_{1,2}$ the group velocity dispersion at FF and SH. The modulation of the second order susceptibility is described by the grating function $G(z)$ which represents a square wave with variable duty cycle and period. If the variations of period and duty cycle are slow compared to the spatial frequency of the grating, we can expand $G(z)$ in Fourier series $G(z) = \chi_0 \Sigma_r g_r(z)\exp(irf(z))$ [$\chi_0 = \omega d_{eff}/(n_m c)$], and, in the spirit of the rotating–wave approximation, we retain only the terms $\pm r$ that are effective (i.e., resonant) to get:[8]

$$\begin{aligned} i\frac{\partial E_1}{\partial z} &= \frac{\beta_1}{2}\frac{\partial^2 E_1}{\partial t^2} - \chi(z)E_1^* E_2, \qquad (2)\\ i\frac{\partial E_2}{\partial z} &= i\delta\frac{\partial E_2}{\partial t} + \frac{\beta_2}{2}\frac{\partial^2 E_2}{\partial t^2} - \chi^*(z)E_1^2, \end{aligned}$$

where $\chi(z) = \chi_0 g_r(z)\exp(irf(z) - i\Delta k z)$. In the case of interest here, the problem of the control of the second harmonic field at output (the target) can be stated as follows: having fixed the FF wave at input, determine the complex function $\chi(z)$ that minimizes the distance between the second harmonic wave at output [$E_2(z = L, t)$]

and the target $[E_{2,target}(t)]$. Once the complex function $\chi(z)$ is obtained, determine the non uniform QPM structure that implements the desired $\chi(z)$.

For real functions, as a measure of the distance between the target and the second harmonic wave at output, we can use the following:

$$J_1 = \frac{1}{2}\int_{-\infty}^{+\infty} \left[E_2(z=L,t) - E_{2,target}(t)\right]^2 dt\,. \qquad (3)$$

Extending to complex functions the algorithm described in,[7] the problem can then be casted in the following way: find the function $\chi(z)$ that minimizes the cost function $J$:[9,10]

$$\begin{aligned} J &= J_1 + J_2 + c.c. \qquad (4)\\ J_2 &= \int_0^L \int_{-\infty}^{+\infty} \lambda_1 \left( \frac{\partial E_1}{\partial z} + i\frac{\beta_1}{2}\frac{\partial^2 E_1}{\partial t^2} - i\chi E_1^* E_2 \right) \\ &+ \lambda_2 \left( \frac{\partial E_2}{\partial z} - \delta\frac{\partial E_2}{\partial t} + i\frac{\beta_2}{2}\frac{\partial^2 E_2}{\partial t^2} - i\chi^* E_1^2 \right) dt dz, \end{aligned}$$

where $J_1$ takes into account the distance from the target, $J_2$ imposes the fulfilment of evolution equations (2) and $\lambda_{1,2}(z,t)$ play the role of Lagrange multipliers.
Setting to zero the functional derivatives of $J$ with respect to $\lambda_1(z,t)$, $\lambda_2(z,t)$, $E_1(z,t)$, $E_2(z,t)$, $E_1(z=L,t)$, $E_2(z=L,t)$ we get six equations.
From the functional derivatives with respect to $\lambda_1$, $\lambda_2$ we get the evolution equations for the FF and the SH components, namely Eqs. (2).
From the functional derivatives with respect to $E_1$, $E_2$ we get the evolution equations for the Lagrange multipliers that read:

$$\begin{aligned} i\frac{\partial \lambda_1}{\partial z} &= -\frac{\beta_1}{2}\frac{\partial^2 \lambda_1}{\partial t^2} - \chi^* \left(\lambda_1^* E_2^* - 2\lambda_2 E_1\right), \\ i\frac{\partial \lambda_2}{\partial z} &= i\delta\frac{\partial \lambda_2}{\partial t} - \frac{\beta_2}{2}\frac{\partial^2 \lambda_2}{\partial t^2} + \chi\lambda_1 E_1^*. \qquad (5) \end{aligned}$$

From the functional derivatives with respect to $E_1(z=L,t)$, $E_2(z=L,t)$ we get the initial condition for the evolution equations of the Lagrange multipliers (to be integrated backward from $z=L$ to $z=0$): $\lambda_1(z=L,t)=0$ and $\lambda_2(z=L,t) = -[E_2(z=L,t) - E_{2,target}(t)]$.
From the functional derivative with respect to $\chi(z)$ we get:

$$\frac{\delta J}{\delta \chi} = \int_{-\infty}^{\infty} \left(-i\lambda_1 E_2 E_1^* + i\lambda_2^* E_1^{2*}\right) dt. \qquad (6)$$

The quantity (6) is used to implement the updating law to determine the optimum $\chi(z)$ in the following iterative algorithm:

1. choose an initial guess for $\chi(z)$;
2. using $\chi(z)$ solve Eqs. (2);
3. using the result obtained in the previous step solve the evolution equations for the Lagrange multipliers (Eqs. (5));
4. update the $\chi(z)$ function: $\chi(z) \leftarrow \chi(z) + \alpha\frac{\delta J}{\delta \chi}$, where $\alpha$ is a suitable constant;
5. if the obtained result is close enough to the target the iterative procedure stops, otherwise it goes back to point 2.

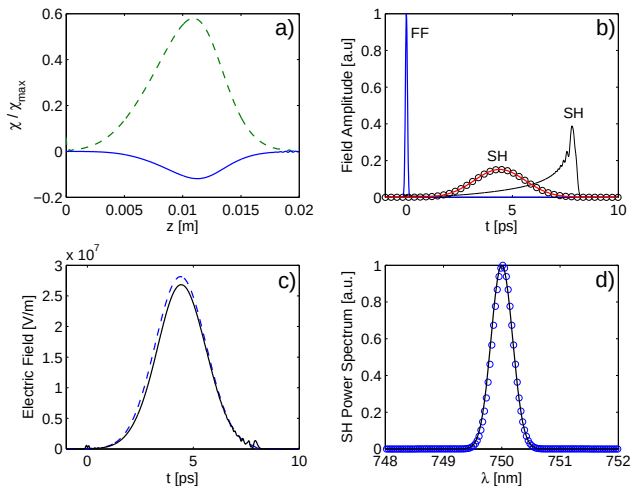


Fig. 1. (Color online) a) Real (solid) and imaginary (dashed) part of the optimal nonlinear coefficient profile normalized to its maximum reachable absolute value $\chi_{max} = \frac{2}{\pi}\chi_0$. b) Input FF (blue thick solid), optimized and desired output SH (solid and circles) and SH output corresponding to a uniform QPM (thin black). c) SH target (dashed) and SH output obtained from the true grating from Eqs.(7-8) (solid). d) Output SH power spectrum (solid) and target (circles): the bandwidth is $0.41\,nm$ ($7.4\,cm^{-1}$).

Once the optimal nonlinear profile is found, the QPM grating can be implemented as follows. Supposing to use a first-order QPM, we consider only the Fourier coefficient of the fundamental harmonic of the grating, i.e. $g_r(z) = g_1(z) = \frac{2}{\pi}\sin(\pi d_c(z))\exp[-i\pi d_c(z)]$, from which we can obtain the duty cycle $d_c(z)$ of the square wave:

$$d_c(z) = \frac{1}{\pi}\arcsin\left(\frac{\pi}{2}\frac{|\chi(z)|}{\chi_0}\right). \qquad (7)$$

The period $\Lambda$ can be obtained form the phase of $\chi(z)$ and considering the variation of the phase of the Fourier coefficient $g_1(z)$ with the duty cycle:

$$\Lambda(z) = 2\pi\left(\Delta k + \frac{d\left[\mathrm{Arg}[\chi(z)] + \pi d_c(z)\right]}{dz}\right)^{-1}. \qquad (8)$$

In order to show the capabilities of the method, we consider periodically poled stoichiometric lithium tantalate (PPSLT) crystals, for which the parameters are $\chi_0 = 1.87{\cdot}10^{-5}\,V^{-1}$, $\delta = -4{\cdot}10^{-10}\,s/m$, $\beta_1 = 0.94{\cdot}10^{-25}\,s^2/m$ and $\beta_2 = 3.7\cdot 10^{-25}\,s^2/m$.

In the first example we consider a $L = 2\,cm$ long crystal and a gaussian transform limited FF input with peak

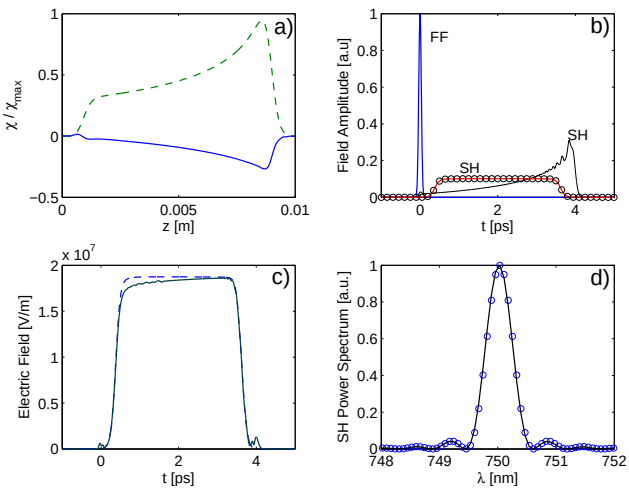


Fig. 2. (Color online) a) Real (solid) and imaginary (dashed) part of the optimal normalized nonlinear coefficient profile. b) Input FF (blue thick solid), optimized and desired output SH (solid and circles) and SH output corresponding to a uniform QPM (thin black). c) SH target (dashed) and SH output obtained from the true grating from Eqs.(7-8) (solid). d) Output SH power spectrum (solid) and target (circles): the bandwidth is $0.45\,nm$ ($8\,cm^{-1}$).

intensity $I = 10\,GW/cm^2$ and full width at half maximum (FWHM) $T_{FF} = 80\,fs$ centered at $\lambda = 1500\,nm$. As a target we choose a SH transform limited gaussian pulse with FWHM $T_{FF} = 2\,ps$ and a desired conversion efficiency of 60%. The results of the iterative algorithm are shown in Fig. 1. Figure 1(a) shows the normalized nonlinear coefficient $\chi(z)$. We can see that both real and imaginary parts are important, since the grating must compensate for the phase that the SH field acquires because of dispersion. Figure 1(b) shows the amplitude of input FF (thick blue line) and output SH fields (thick red line) compared to the target (black circles): the agreement is perfect (after 100 iterations the relative error is less than $10^{-4}$, with a total CPU time of approximatively two minutes). For comparison is reported the output of the uniform QPM grating (thin black line), which has the typical shape of a steep leading-edge and a long oscillating tail. Figure 1(c) shows the SH output amplitude obtained from the simulation of the real QPM grating corresponding to Eqs.(7-8): the curve fits quite well the target, confirming the validity of the rotating-wave approximation and the slow variation of period and duty cycle. Finally Fig. 1(d) shows the output SH spectrum, which confirms that the output is transform limited, and its bandwidth is $0.41\,nm$ ($7.4\,cm^{-1}$).

As a second example we consider an $L = 1\,cm$ crystal and a gaussian transform limited FF input with peak intensity of $I = 10\,GW/cm^2$ and FWHM of $T_{FF} = 55\,fs$ centered at $\lambda = 1500\,nm$. As a target we choose a SH transform limited flat top pulse of FWHM $T_{FF} = 3\,ps$ and a desired conversion efficiency of 60%. The results of the iterative algorithm are shown in Fig. 2. Figure 2(a) shows the normalized nonlinear coefficient $\chi(z)$. Note the trapezoidal profile, which compensate for the strong FF depletion along propagation. Figure 2(b) shows the amplitude of input FF (thick blue line) and output SH fields (thick red line) compared to the target (black circles): also in this case the agreement is perfect (the relative error is less than $10^{-4}$). For comparison is reported the output of the uniform QPM grating (thin black line). The strong difference between the uniform and non uniform QPM witnesses that the pump depletion plays a fundamental role in our case: in fact in the low-depletion limit, the output of a uniform QPM grating would be a flat top pulse. Figure 2(c) shows the good agreement between SH output amplitude obtained from the simulation of the real QPM grating corresponding to Eqs.(7-8) and the target. Finally Fig. 2(d) shows the output SH spectrum, which confirms that the output is transform limited, and its bandwidth is $0.45\,nm$ ($8\,cm^{-1}$).

In conclusion an optimal control technique has been used to mould optical fields obtained from second harmonic generation of femtosecond infrared pulses in order to obtain picosecond visible pulses of the desired amplitude, phase profile and carrier wavelength. In our work we account for both group velocity dispersion and pump depletion and give the rules for the practical implementation of a non uniform QPM structure. Our results suggest a valuable means for generating the visible pulses needed by several applications in a way that is simpler and cheaper than the state of art. Moreover the method described here is quite general and can be exploited in other areas of optics whenever an optical pulse with special characteristics is required.

## References


1. D. W. McCamant, P. Kukura, S. Yoon, and R. A. Mathies, Rev. Sci. Instrum. **71,** 4971 (2004).
2. R. Ellingson and C. Tang, Opt. Lett. **18,** 438 (1993); E. Cheung, K. Koch, and G. Moore, Opt. Lett. **19,** 1967 (1994); X. Zhang, J. Hebling, J. Kuhl, W. Ruhle, and H. Giessen, Opt. Lett. **26,** 2005 (2001).
3. M. Ebrahimzadeh, M. H. Dunn, and F. Akerboom, Opt. Lett. **14,** 560 (1989); V. Petrov, F. Seifert, and F. Noack, Appl. Opt. **33,** 6988 (1994).
4. K. Moutzouris, F. Adler, F. Sotier, D. Trautlein, and A. Leitenstorfer, Opt. Lett. **31,** 1148 (2006).
5. M. A. Arbore, O. Marco, and M. M. Fejer, Opt. Lett. **22,** 865 (1997); G. Imeshev, A. Galvanauskas, D. Harter, M. A. Arbore, M. Proctor, and M. M. Fejer, Opt. Lett. **23,** 864 (1998).
6. U. K. Sapaev and D. T. Reid, Opt. Exp. **13,** 3264 (2005).
7. R. Buffa, Opt. Lett. **27,** 1058 (2002).
8. O. Bang, C. B. Clausen, P. L. Christiansen, and L. Torner, Opt. Lett. **24,** 1413 (1999).
9. I. Serban, J. Werschnik, and E. K. U. Gross, Phys. Rev. A **71,** 053810 (2005).
10. A. Kaiser, and V. May, Chemical Physics **320,** 95 (2006).